Influence of adhesion-promoting glycolipids on the structure and stability of solid-supported lipid double-bilayers

Lukas Bange,[†] Tetiana Mukhina,[†] Giovanna Fragneto,[‡,§] Valeria Rondelli,[*,¶] and Emanuel Schneck[*,†]

†*Institute for Condensed Matter Physics, TU Darmstadt, Hochschulstraße 8, 64289 Darmstadt, Germany*

‡*Institut Laue-Langevin, Grenoble, France*

¶*Department of Medical Biotechnology and Translational Medicine, Università degli Studi di Milano, Italy*

§*The European Spallation Source, ERIC, Lund, Sweden*

E-mail: valeria.rondelli@unimi.it; emanuel.schneck@pkm.tu-darmstadt.de

Abstract

Glycolipids have a considerable influence on the interaction between adjacent biomembranes and can promote membrane adhesion trough favorable sugar-sugar "bonds" even at low glycolipid fractions. Here, in order to obtain structural insights into this phenomenon, we utilize neutron reflectometry in combination with a floating lipid bilayer architecture that brings two glycolipid-loaded lipid bilayers to close proximity. We find that selected glycolipids with di-, or oligosaccharide headgroups affect the inter-bilayer water layer thickness and appear to contribute to the stability of the double-bilayer architecture by promoting adhesion

of adjacent bilayers even against induced electrostatic repulsion. However, we do not observe any redistribution of glycolipids that would maximize the density of sugar-sugar contacts. Our results point towards possible strategies for the investigation of interactions between cell surfaces involving specific protein-protein, lipid-lipid, or protein-lipid binding.

Introduction

Glycolipids influence the behavior of lipid bilayers in various ways that have far-reaching consequences for the functions of biological membranes and cells.[1–4] Among the important aspects is the impact of glycolipids on interactions with other bilayers.[5,6] For example, for high glycolipid fractions, the hydration repulsion governing the thickness of the inter-bilayer water layer is substantially reduced with respect to commonly studied phosphocholine (PC) lipid bilayers, such that spontaneous membrane stack formation is promoted.[7–9] But already low fractions of glycolipids can significantly strengthen membrane adhesion via weak sugar-sugar "bonds", as was found in experimental studies utilizing micropipetting,[10,11] the surface force apparatus,[12] as well as x-ray and neutron scattering techniques,[13,14] and later on in a simulation-based study.[15] Recently, additional features of glycolipid-loaded bilayers were identified that have to do with preferential sugar-sugar interactions. For example, certain glycolipids with mono-, di-, and oligosaccharide headgroups can enhance the chain ordering in binary glycolipid/phospholipid mixtures,[16–18] and direct carbohydrate-carbohydrate interactions can drive the insertion of biosurfactants into lipid membranes.[19] While most of these phenomena have been observed for comparatively simple synthetic glycolipids, one may expect that the underlying mechanisms apply equally to biological membranes with their diverse and chemically more complex glycosphingolipids, such as gangliosides with their numerous functions in protein regulation and lateral segregation.[20,21] Among them, the ganglioside GM1 is particularly abundant in the nervous system and accounts for 80% of all glycans in the brain.[22]

So far, structural investigations on the role of glycolipids in membrane adhesion have been performed mainly with lipid multibilayers,[13,14,23] which are hardly suited to provide sufficiently detailed structural information in the direction perpendicular to the surface. Structural detail is however required to investigate the distribution of lipid species across the bilayer or to investigate asymmetrical interaction scenarios with different glycolipid types or densities in the two opposing lipid surfaces.

Solid supported lipid bilayers are versatile and well established platforms for membrane-biophysical studies and for the structural characterization of lipid bilayers in the direction perpendicular to the surface by neutron reflectometry (NR).[24] To this end, "floating lipid bilayers" (FLB), supported by lipid mono- or bilayers and prepared via the Langmuir-Blodgett/Langmuir-Schaefer (LB/LS) techniques,[25–29] are particularly useful because they avoid perturbation of the bilayer through strong (and non-physiological) interactions with a bare solid support.

Here we use NR to investigate the influence of glycolipids with the documented ability to form inter-bilayer sugar-bonds on the structure and stability of FLBs that bring two bilayers into proximity. The studied glycolipids with di-, tri-, or pentasaccharide headgroups are found to have impacts on the inter-bilayer water layer thickness, and most of them appear to contribute to the FLB stability although they do not accumulate on the bilayer face on which inter-bilayer sugar-bonds can be formed.

Materials and methods

Materials

Chloroform (purity $\geq$ 99.9% [Warning: toxic on incorporation, inhalation, skin, and eye contact; use under fume hood and/or with suitable personal protection]), methanol (purity $\geq$ 99.9% [Warning: toxic on incorporation, inhalation, skin, and eye contact; use under fume hood and/or with suitable personal protection]), D_2O (isotopic purity $\geq$ 99.8), NaCl,

and $CaCl_2$ were purchased from Sigma-Aldrich and used without further purification. GM1 ganglioside was purchased from Merck. Double deionized ultrapure water (resistivity: 18.2 MΩ·cm) was obtained from a water purification station (Elga, Purelab classic). Silicon single crystal blocks, 50 mm × 50 mm × 10 mm in size, polished on one large (111) face and terminated with a thin layer of native silicon oxide, were purchased from Sil'tronix (Archamps, France).

The phospholipids 1,2-distearoyl-sn-glycero-3-phosphocholine (DSPC) and 1,2-dipalmitoyl-sn-glycero-3-phosphocholine (DPPC), both in hydrogenous and chain-perdeuteraded forms, were purchased from Avanti Polar Lipids (Alabaster, AL). The glycolipids N-hexadecanoyl-lactosyl-ceramide (LacCer-sat) and N-hexadecanoyl-ceramide-trihexoside (Trihexo-sat) were purchased from Matreya (State College, PA). The glycolipids were available with C16 and C18 chains (LacCerC16, LacCerC18, TrihexoC16), TrihexoC18) to be able to match both the chains of DSPC and DPPC, as detailed in Fig. 1.

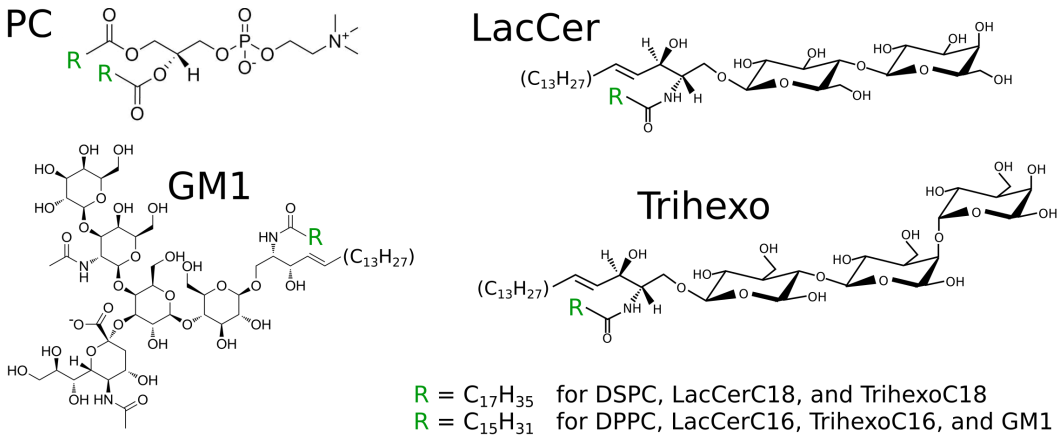

Figure 1: Chemical structures of all lipids investigated: DSPC, DPPC, Lactosyl-Ceramide (LacCer), Trihexoside-Ceramide (Trihexo), Ganglioside M1 (GM1).

Sample preparation

All glassware and sample vials were washed with chloroform before use. Lipid solutions were prepared by dissolving lipid powder at a concentration of 1 mg/mL in chloroform or a mixture of chloroform and methanol (2:1 by volume), for phospholipid or glycolipids, respectively.

Mixed solutions were then obtained by mixing these solutions in suitable volume ratios. Silicon-matched water (SMW) was obtained by mixing H_2O and D_2O in the volume ratio 1.63:1. The silicon blocks were first cleaned with the organic solvents chloroform, acetone, and ethanol and subsequently treated in a plasma cleaner for 10 min.

FLBs were prepared at 20 °C by the sequential deposition of individual lipid monolayers onto the surfaces of the blocks with the Langmuir-Blodgett (LB) / Langmuir-Schaefer (LS) techniques. Teflon Langmuir troughs were used for this purpose, either by Nima Technology (Coventry, UK) or by Riegler & Kirstein (Potsdam, Germany). Starting with the bare block inside the aqueous medium, the first three transfers were performed with LB, by moving the block first out, then in, and then out again, at a speed of 6 mm/min. Only the last transfer was performed with LS, and the block then remained inside the NR measurement cell. Before each transfer, a lipid monolayer at the air/water was prepared by spreading a suitable amount of lipid solution, allowing 10 min for complete evaporation, and compressing the monolayer to the desired pressure of $\pi = 40$ mN/m, which was kept constant during the transfers through barrier movements. Ellipsometry experiments were carried out on independent samples after the first and the third transfer step.

Ellipsometry

As described in an earlier publication,[30] from which the following paragraph is partially reproduced, ellipsometry enables the characterization of interfacial layers in terms of refractive indices and thicknesses. The method is based on the change in the polarization state of light upon reflection from the surface. For a given refractive index n, the change depends on the layer thickness and is quantified in terms of the phase difference Δ and the amplitude ratio Ψ encoded in the ratio between the complex reflection coefficients R_s and R_p for s and p polarizations, respectively:[31]

$$R_\mathrm{p}/R_\mathrm{s} = \tan\Psi e^{-i\Delta} \tag{1}$$

Ellipsometry measurements were carried out with the same silicon blocks which where later used for the NR experiments and have a thin ($\approx$ 10 Å) layer of native oxide on their surface. The measurements were performed at an incident angle of 70° with an Optrel Multiskop ellipsometer working with a wavelength $\lambda_{\mathrm{elli}} = 632.8$ nm. Silicon has the complex refractive index $n_{\mathrm{Si}} = 3.885–0.018\mathrm{i}$.[32] As refractive index of the silicon oxide we assumed the $n_{\mathrm{oxi}} = 1.47$ as determined earlier.[30] For the hydrated organic layers we assume $n_{\mathrm{org}} = 1.5$, consistent with earlier reports on organic materials.[33,34]

NR experiments

NR was performed with the reflectometer FIGARO[35] of Institut Laue-Langevin (ILL, Grenoble, France) as generally described in our earlier work[36] from which the following paragraph is partially reproduced. All measurements were carried out using "solid/liquid cells". After passing through the silicon block, the incident beam hits the solid-liquid interface with an angle θ and the beam portion reflected at the same angle is collected. The reflectivity, that is, the intensity ratio R between reflected and incident beams, with wave vectors $\vec{k}_{\mathrm{i}}$ and $\vec{k}_{\mathrm{f}}$, respectively, is recorded as a function of $q_z = |\vec{k}_{\mathrm{f}} - \vec{k}_{\mathrm{i}}| = (4\pi/\lambda)\sin\theta$, the scattering vector component perpendicular to the interface (see Figure 1B). Here, λ denotes the neutron wavelength. The measurements were conducted in the time-of-flight mode using two fixed incident angles $\theta_1 = 1.0°$ and $\theta_2 = 3.5°$. The wavelength range was 2 Å $\leq \lambda \leq$ 20 Å. The q_z-resolution in terms of the relative width $\Delta q_z/q_z$ corresponds to the finite angular and wavelength resolutions, is q_z-dependent, and varied between 7% and 10%. While modeling experimental reflectivity curves, the finite experimental resolution was taken into account by convoluting the initial reflectivity curves, calculated for the case of infinite resolution, with Gaussian functions representing the resolution function of the experiments. The curves $R(q_z)$ depend on the interfacial scattering length density (SLD) distribution of all chemical

components j having their characteristic and known SLDs ρ_j:

$$\rho_j = \frac{1}{v_j} \sum_k N_k^j b_k \tag{2}$$

, where b_k is the coherent scattering length of an atomic nucleus of type k and N_k^j is the number of such nuclei in component j per volume v_j. The SLD strictly refers to the anhydrous chemical components and their solvent-excluded volume. With that, the xy-averaged volume fraction profiles of all components in the direction (z) perpendicular to the surface can be reconstructed from $R(q_z)$. To avoid ambiguities in this procedure, and to enhance sensitivity to the chemical components of interest, a technique called contrast variation is applied, which is possible because of the large difference of the scattering length of the hydrogen isotopes H and D. The SLD of the aqueous medium is varied by replacing H_2O with D_2O or defined H_2O/D_2O mixtures with a desired SLD. To this end, we use three H_2O/D_2O mixtures, pure H_2O (ρ_W = -0.56 $\cdot$ 10^{-6} Å^{-2}), pure D_2O (ρ_W = 6.35 $\cdot$ 10^{-6} Å^{-2}), and a mixture matching the SLD of the silicon substrate (SMW, ρ_W = 2.07 $\cdot$ 10^{-6} Å^{-2}). Minor deviations in ρ_W can occur because of incomplete exchange of the aqueous medium inside the cell during the rinsing procedure. This was accounted for by allowing for small variations in ρ_W in the data analysis. Moreover, in certain samples, phospholipids with deuterated hydrocarbon chains (d-phospholipids) were introduced to enhance the SLD contrast against glycolipids with unmodified (hydrogenous) hydrocarbon chains. Most of the chemical components of which the samples are composed have constant SLDs. This applies to crystalline silicon (ρ_{Si} = 2.07 $\cdot$ 10^{-6} Å^{-2}), silicon oxide (ρ_{oxi} = 3.47 $\cdot$ 10^{-6} Å^{-2}), hydrogenous lipid hydrocarbon chains (ρ_{hHC} = -0.4 $\cdot$ 10^{-6} Å^{-2}), deuterated lipid hydrocarbon chains (ρ_{dHC} = 7.1 $\cdot$ 10^{-6} Å^{-2}), and phospholipid headgroups (ρ_{PHG} = 1.75 $\cdot$ 10^{-6} Å^{-2}), as was established earlier.[30,37] Because of the dynamic H/D exchange of "labile" hydrogens, however, the SLD of the glycolipids'

saccharide headgroups, ρ_{GHG}, depends on the SLD ρ_{W} of the aqueous medium:[38]

$$\rho_{\mathrm{GHG}} = A + B\rho_{\mathrm{W}} \tag{3}$$

, where $A = 2.10 \cdot 10^{-6}$ Å^{-2} and $B = 0.258$ for LacCer, $A = 2.22 \cdot 10^{-6}$ Å^{-2} and $B = 0.270$ for Trihexo, and $A = 2.09 \cdot 10^{-6}$ Å^{-2} and $B = 0.258$ for GM1 (see Supporting Information).

NR data analysis

The reflectivity curves obtained with samples of the same kind but under different SLD contrast conditions (H_2O/D_2O mixtures and lipid deuteration schemes) were simultaneously described with a common model. This model (see Fig. 2) is based on the volume fraction profiles, $\phi_j(z)$, of all chemical components perpendicular to the interface and simultaneously describes the reflectivity curves of a sample for all measurement conditions (Fig. 3), that is, for all H_2O/D_2O mixtures and for samples based on h-phospholipids and on d-phospholipids. The chemical components are silicon (Si), silicon oxide (oxi), phospholipid hydrocarbon chains (PHC), phospholipid headgroups (PHG), glycolipid hydrocarbon chains (GHC), glycolipid headgroups (GHG), and water (W). The SLD profile $\rho(z)$ for each condition then follows as:

$$\rho(z) = \rho_{\mathrm{Si}}\phi_{\mathrm{Si}}(z)+\rho_{\mathrm{oxi}}\phi_{\mathrm{oxi}}+\rho_{\mathrm{xHC}}\phi_{\mathrm{PHC}}(z)+\rho_{\mathrm{hHC}}\phi_{\mathrm{GHC}}(z)+\rho_{\mathrm{PHG}}\phi_{\mathrm{PHG}}(z)+\rho_{\mathrm{GHG}}\phi_{\mathrm{GHG}}(z)+\rho_{\mathrm{W}}\phi_{\mathrm{W}}(z) \tag{4}$$

, where $\rho_{\mathrm{xHC}} = \rho_{\mathrm{hHC}}$ for h-phospholipids and $\rho_{\mathrm{xHC}} = \rho_{\mathrm{dHC}}$ for d-phospholipids. The distance measured perpendicular to the surface is denoted with z, where $z = 0$ is arbitrarily defined as the interface between the silicon and the oxide layer. By construction, the sum of

all volume fractions in the model amounts to unity at each z-position:

$$\sum_j \phi_j(z) \equiv 1 \tag{5}$$

For the volume fraction profiles we use a layer description determined by a set of adjustable parameters and in the spirit of our earlier work.[30,36] Silicon oxide, lipid HC and HG, as well as the water layers below and between the lipid bilayers are described as homogeneous layers with adjustable thickness (d) and roughness (σ) parameters. Here, $d_{\mathrm{W}}^{\mathrm{SiBL}}$ is the thickness of the thin hydration layer between the silicon oxide and the headgroups of the proximal bilayer and d_{W} is the thickness of the water layer between the headgroup regions of the two bilayers. An idealized (roughness-free), schematic illustration of the model is shown in Fig. 2 A. The addition of a distinct layer for the "methyl dip", which is essential to model x-ray reflectivity from lipid bilayers,[39] was found to be unnecessary, in line with earlier reports.[40] The oxide layer is allowed to have a finite water fraction $\phi_{\mathrm{W}}^{\mathrm{oxi}}$, which represents both internal hydration and silanols.[30] In order to reduce the number of adjustable model parameters it is convenient to quantify the amount per area of each component by its equivalent thickness

$$D_j = \int_{-\infty}^{\infty} \phi_j(z) dz \tag{6}$$

, which coincides with the thickness of an equivalent layer entirely composed of that component. For a monolayer with glycolipid fraction x_{GL} and phospholipid fraction $x_{\mathrm{PL}} = 1 - x_{\mathrm{GL}}$ we obtain $D_{\mathrm{GHC}} = x_{\mathrm{GL}} D_{\mathrm{HC}}$ and $D_{\mathrm{PHC}} = (1 - x_{\mathrm{GL}}) D_{\mathrm{HC}}$, when the HC of glycolipids and phospholipids are of the same type and volume. Here, the chain volumes are $v_{\mathrm{HC}} = 980$ Å^3 for a pair of C18 chains and $v_{\mathrm{HC}} = 870$ Å^3 for a pair of C16 chains. Moreover, HGs and pairs of HCs always occur in a 1:1 stoichiometry, requiring that the respective equivalent thicknesses are coupled, $D_{\mathrm{PHG}} = D_{\mathrm{PHC}} v_{\mathrm{PHG}} / v_{\mathrm{HC}}$ and $D_{\mathrm{GHG}} = D_{\mathrm{GHC}} v_{\mathrm{GHG}} / v_{\mathrm{HC}}$. Here, the volume of the phospholipid headgroup is $v_{\mathrm{PHG}} = 340$ Å^3 and that of the glycolipid headgroup is $v_{\mathrm{GHG}} = 419$ Å^3 for LacCer, $v_{\mathrm{GHG}} = 551$ Å^3 for Trihexo (see Supporting Information and

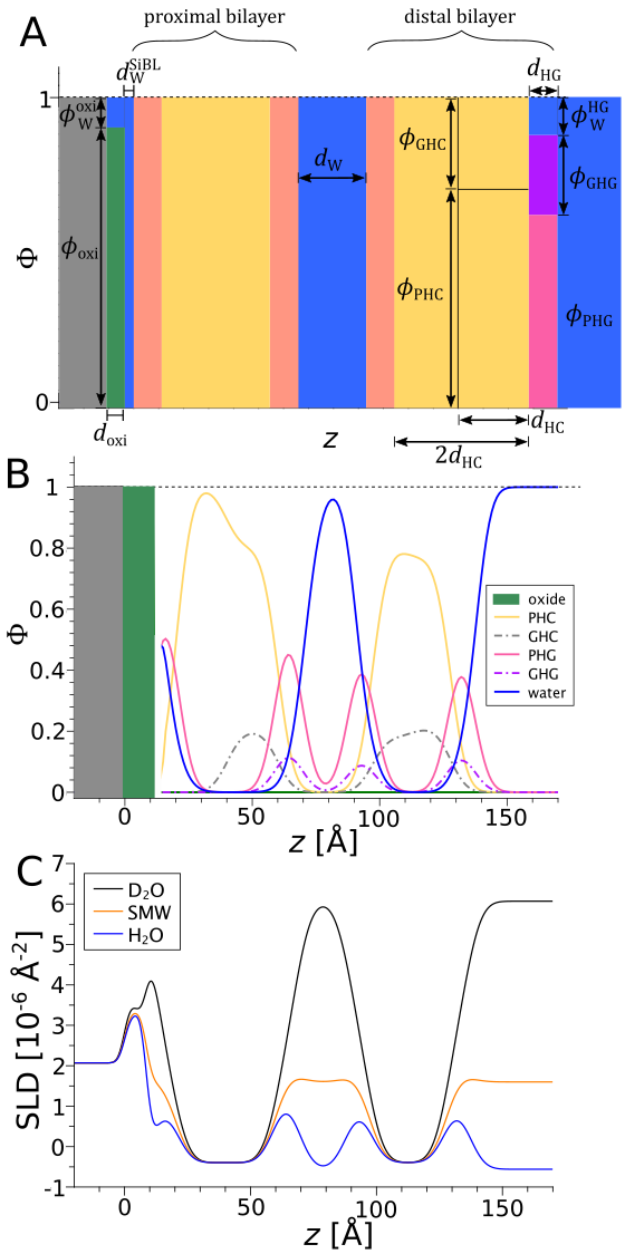

Figure 2: (A) Roughness-free description of the distributions of all chemical components in terms of the thickness and volume fraction parameters of defined layers. The indicated parameters are defined in the text. (B) Resulting volume fraction profiles for a parameter set that describes a PC/Trihexo FLB at 50°C simultaneously in all H_2O/D_2O mixtures and with both phospholipid deuteration schemes. PHC: phospholipid hydrocarbon chains, PHG: phospholipid headgroups, GHC: glycolipid hydrocarbon chains, GHG: glycolipid headgroups. (C) Corresponding SLD profiles for the h-phospholipid-based PC/Trihexo FLB in three different H_2O/D_2O mixtures (D_2O, SMW, and H_2O).

ref.[41]), and $v_{\mathrm{GHG}} = 1000$ Å^3 for GM1.[42]

The HC chains are hydrophobic and therefore the HC layers are safely assumed to be free of water (see Fig. 2 A), in which case the equivalent thickness simply coincides with the layer thickness, $D_{\mathrm{HC}} = d_{\mathrm{HC}}$. In contrast, the equivalent thickness of headgroups is smaller than the thickness of the hydrated HG layer, $D_{\mathrm{HG}} = d_{\mathrm{HG}}(1 - \phi_{\mathrm{W}}^{\mathrm{HG}})$, where $\phi_{\mathrm{W}}^{\mathrm{HG}}$ is the water fraction of the HG layer (Fig. 2 A). For a given set of parameters D_{HC}, x_{GL}, and d_{HC}, the water fraction thus follows as $\phi_{\mathrm{W}}^{\mathrm{HG}} = 1 - [D_{\mathrm{HC}}/(d_{\mathrm{HG}} v_{\mathrm{HC}})] \cdot [(1 - x_{\mathrm{GL}}) v_{\mathrm{PHG}} + x_{\mathrm{GL}} v_{\mathrm{GHG}}]$.

In the model, PHGs and GHGs are pooled in a single layer of thickness d_{HG}. This simplification is practicable because the SLD contrast between water and the GHGs, due to the pronounced H/D exchange, is quite weak and because x_{GL} is comparatively low. As a consequence, the reflectivity curves are not very sensitive to the GHG distribution. Indeed, as shown in the Supporting Information (Fig. S7), the fit remains virtually unchanged when an extra parameter for the GHG layer extension is introduced and varied within a plausible range. To further reduce the number of free model parameters, the distal bilayer is assumed to be symmetrical with regard to the HC and HG thickness and roughness parameters of the constituting monolayers, but not with regard to the glycolipid fraction in each monolayer. The two HG layers of the proximal bilayer have independent thickness parameters because their environment is strongly asymmetrical and because they have very different composition as imposed by the composition of the sequentially transferred monolayers.

Turning to the distribution of glycolipids over the two monolayers of a bilayer, we generally account for the possibility of an exchange between the two monolayers of a fluid bilayer through lipid flip-flop or other mechanisms to the same effect. The glycolipid fractions x_{GL} in the two monolayers, termed $x_{\mathrm{GL}}^{\mathrm{in}}$ and $x_{\mathrm{GL}}^{\mathrm{out}}$, are therefore assumed as variable but mutually coupled as imposed by the known total glycolipid fraction $x_{\mathrm{GL}}^{\mathrm{BL}}$ in the bilayer,

$$x_{\mathrm{GL}}^{\mathrm{in}} = 2 f_{\mathrm{in}} x_{\mathrm{GL}^{\mathrm{BL}}} \tag{7}$$

$$x_{\mathrm{GL}}^{\mathrm{out}} = 2(1 - f_{\mathrm{in}}) x_{\mathrm{GL}^{\mathrm{BL}}} \tag{8}$$

, such that we are left with only one independent parameter $f_{\mathrm{in}} \in (0, 1)$ for the glycolipid distribution in the distal bilayer when it is in the fluid state.

Fig. 2 B shows the volume fraction profiles of all chemical components resulting from this modeling approach for a suitable set of parameters and after application of all interfacial roughnesses regarding the oxide and lipid layers. Following previous work[43] the thermal fluctuations of the two bilayers were considered by convolution of the corresponding volume fractions with Gaussian functions of widths $\sigma_{\mathrm{fluc}}^{\mathrm{prox}}$ and $\sigma_{\mathrm{fluc}}^{\mathrm{dist}}$ for the proximal and distal bilayers, respectively, in addition to bilayer-internal roughness parameters, which were all fixed at $\sigma_{\mathrm{int}} = 2$ Å. The consequence of this convolution for the volume fraction profiles is illustrated in Fig. S1 of the Supporting Information. While fixing σ_{int} at a finite value does not actually improve the model, it does reduce the number of free parameters for the fit. Here, a value of 2 Å was primarily chosen to realistically reflect the SLD gradient due to variations of the chemical composition along the molecular structure. A less realistic choice of σ_{int} would have resulted in the same fit quality, albeit in under- or overestimated values of $\sigma_{\mathrm{fluc}}^{\mathrm{prox}}$ and $\sigma_{\mathrm{fluc}}^{\mathrm{dist}}$.

Fig. 2 C shows the resulting SLD profiles according to Eq. 4 for a sample with all hydrogenated hydrocarbon chains in three different H_2O/D_2O mixtures, D_2O, SMW, and H_2O.

The final aspect to be considered is the surface coverage. The most common approach to modeling incomplete bilayer coverage is to multiply all lipid-related volume fractions with a coverage fraction $f_{\mathrm{BL}} \in (0, 1)$ and filling up the rest with water, that is, replacing $\phi_j(z)$ with $\phi'_j(z) = f_{\mathrm{BL}} \phi_j(z)$ and $\phi_{\mathrm{W}}(z)$ with $\phi'_{\mathrm{W}}(z) = \phi_{\mathrm{W}}(z) + (1 - f_{\mathrm{BL}}) \sum_j \phi_j(z)$ in Eq. 4 for $j \in \{\mathrm{PHC}, \mathrm{GHC}, \mathrm{PHG}, \mathrm{GHG}\}$. This treatment, termed *coherent* treatment in the following, is valid when bilayer heterogeneities are on length scales much smaller than the in-plane coherence length of the probing neutron beam. Another way of dealing with incomplete bilayer coverage is to model the SLD profiles and reflectivity curves of covered and uncovered surface regions independently and then represent the experimental reflectivity curves as weighted sum of the model reflectivities from the covered and uncovered regions. This

treatment is called *incoherent* treatment in the following because it is valid when bilayer heterogeneities are on length scales much larger than the in-plane coherence length of the probing neutron beam. In this case, the reflectivity is modeled as

$$R(q_z) = f_{\mathrm{BL}}^{\mathrm{dist}} R_{\mathrm{2BL}}(q_z) + (f_{\mathrm{BL}}^{\mathrm{prox}} - f_{\mathrm{BL}}^{\mathrm{dist}}) R_{\mathrm{1BL}}(q_z) + (1 - f_{\mathrm{BL}}^{\mathrm{prox}}) R_{\mathrm{bare}}(q_z) \tag{9}$$

, where $f_{\mathrm{BL}}^{\mathrm{prox}}$ and $f_{\mathrm{BL}}^{\mathrm{dist}}$ are the coverage fractions of the proximal and distal bilayer, respectively, with $f_{\mathrm{BL}}^{\mathrm{prox}} \geq f_{\mathrm{BL}}^{\mathrm{dist}}$, and R_{bare}, R_{1BL}, and R_{2BL} are the reflectivities from the uncovered (bare) regions of the sample, from the regions covered with only the proximal bilayer, and from the regions covered with both bilayers, respectively. Note that Eq. 9 by construction fulfills the normalization condition, $f_{\mathrm{BL}}^{\mathrm{dist}} + (f_{\mathrm{BL}}^{\mathrm{prox}} - f_{\mathrm{BL}}^{\mathrm{dist}}) + (1 - f_{\mathrm{BL}}^{\mathrm{prox}}) = 1$.

To simultaneously fit the adjustable parameters of the common model to a set of experimental reflectivity curves (see Figs. 3 and 6), we started from an "educated guess" of initial parameter values and first calculated the interfacial SLD profiles corresponding to each condition. In the next step, we calculated the corresponding reflectivity curves using dynamical reflection theory. To this end, the profiles were discretized into hundreds of thin slabs of 1 Å thickness and of constant SLD. The q_z-dependent intensities were then calculated via application of Fresnel's reflection laws at each slab/slab interface using the iterative procedure of Parratt.[44] The best-matching parameters stated in the text and summarized in Tables 2 and 3 correspond to the minimal χ^2-deviation between simulated and experimental intensities. Estimates of the statistical parameter errors, e.g. corresponding to the 95% (two-sigma) confidence interval, are valid only within the framework of a "perfect model", characterized by a reduced χ^2 close to unity[45] and typically greatly underestimate the real uncertainty. In view of significant additional contributions due to systematic errors, much larger error estimates are therefore provided instead in the tables next to the parameter values. They approximately reflect the variation of the obtained parameters throughout the evolution and refinement of the above-described model description, i.e., they reflect the robustness of the parameters with respect to the model, and we therefore consider them more meaningful.[30]

Results and discussion

The floating lipid bilayer samples were prepared through a combination of the LB and LS transfer techniques to sequentially deposit four lipid monolayers onto the initially bare silicon substrates (see Methods section for further details). While the first monolayer was always of pure phospholipid, layers 2-4 contained defined fractions of glycolipids,[14,46] either LacCer, Trihexo, or GM1 (see Fig. 1). LacCer and Trihexo were previously shown to stabilize bilayer adhesion even against induced electrostatic repulsion.[14] The glycolipid fractions in layers 2-4 were $x_{\mathrm{GL}}^{\mathrm{BL}} = 0.2$ (20 mol%) for LacCer and Trihexo and 5 mol% or 10 mol% for GM1. Layers 1-2 were based on DSPC (forming densely-packed and chain-ordered layers up to 55 °C), while layers 3-4 were based on DPPC (chain melting temperature 41 °C). In order to match the chain lengths of the matrix phospholipids, C_{18}-glycolipids ($\mathrm{LacCerC_{18}}$ or $\mathrm{TrihexoC_{18}}$) were used for layer 2 and C_{16}-glycolipids ($\mathrm{LacCerC_{16}}$ or $\mathrm{TrihexoC_{16}}$) for layers 3 and 4. In the following, PC-based FLBs containing LacCer, Trihexo, or GM1 glycolipids will be referred to as "PC/LacCer FLB", "PC/Trihexo FLB", and "PC/GM1 FLB", respectively. The glycolipid-free reference system will be simply called "PC FLB".

We were primarily interested in the stability of glycolipid-containing FLB samples, in the influence of glycolipids on the thickness of the water layer between the two bilayers when linked together trough attractive sugar-sugar interactions, and on the amplitude of the thermal fluctuations as manifested in the associated roughness parameter. Moreover, we were interested in whether preferential sugar-sugar interactions would accumulate glycolipids at the inner leaflet of the outer bilayer, via flip-flop mechanisms known for sterols and phospholipids[47] or other mechanisms to the same effect, e.g., diffusion through defects. In the following we will present our results on the above-mentioned aspects by describing the samples first on a macroscopic scale by ellipsometry and then on a detailed structural level by NR.

Ellipsometry

Ellipsometry experiments allowed us to identify conditions under which the sequential transfer of the lipid monolayers onto the silicon surfaces was most successful. Reproducibly excellent bilayer coverage was only achieved when completely dipping the solid substrates under water during LB transfers, which was achieved with a modified holder for the solid substrate. Table 1 exemplarily summarizes the ellipsometric angles Δ and Ψ obtained with a bare silicon surface, the surface after the first LB transfer, and the surface after the third and last LB transfer, together with the corresponding overall lipid layer thicknesses D_{lip} determined in the modeling procedure (see Methods section). Note that the second and third transfers are the critical steps in the sample preparation and that the samples are stable in air only after uneven transfer numbers, that is, when lipid hydrophobic portions are exposed to air. It is seen that D_{lip} is approximately proportional to the number of monolayers transferred and an absolute value of ≈ 90 Å for the whole architecture is realistic when assuming roughly 25 Å per monolayer plus the hydration water. Moreover, the thickness variation over the surface is remarkably small (see Supporting Information Table S2), indicating excellent surface coverage with three monolayers. However, when incomplete coverage occurred nonetheless, then distinct mm-sized regions covered with only one transferred monolayer were found (as seen from the ellipsometric angles), such that only one bilayer would result after the final (non-critical) LS transfer. This observation is in contrast to the usual picture of having continuous bilayers with water-filled nanoscale defects.

Table 1: Ellipsometric angles Δ and Ψ (average $\pm$ standard deviation over the sample surface) and corresponding overall lipid layer thickness D_{lip}. System: Pure PC lipids in all monolayers. [a]Values assuming $D_{\mathrm{oxi}} \approx 10$ Å (see NR results below).

sample	Δ [°]	Ψ [°]	D_{lip} [Å]
bare block	176.4[a]	10.6[a]	-
after 1st transfer	166.0	10.8	35
after 3rd transfer	150.7 $\pm$ 0.2	11.51 $\pm$ 0.06	92 $\pm$ 1

Neutron reflectometry

The samples were first characterized at a controlled temperature of 25°C and then heated to 50°C such that the proximal (supporting) bilayer remained in the chain-crystalline state while the distal bilayer assumes the biologically most relevant fluid phase. This can be safely assumed because even for directly solid-supported bilayers, where interactions with the surface are strong, the transition temperature is shifted only by few degrees upwards.[48] For the distal bilayer, which is separated from the proximal bilayer by a considerable water layer, the transition temperature has been reported to be even slightly lower than in multilamellar bulk phases.[49] Indeed, as presented further below, the NR data confirmed the intended phase states for both bilayers at both temperatures. Fig. 3 shows an exemplary set of reflectivity curves obtained at 50°C with a PC/Trihexo FLB. The figure contains data from samples with chain-hydrogenous (panel A) and chain-deuterated (panel B) phospholipids (h-phospholipids and d-phospholipids, respectively) and from three H_2O/D_2O mixtures (H_2O, SMW, D_2O). Note that the samples with h- and d-phospholipids were prepared independently but otherwise can be considered to be of the same kind. The solid lines indicate the simulated reflectivity curves corresponding to a common model described in the Methods section and illustrated in Fig. 2. All system-intrinsic parameters like membrane and water layer thicknesses, roughnesses, and parameters specifying the distribution of glycolipids over membrane leaflets are assumed to be identical for all six curves obtained with two samples and three H_2O/D_2O mixtures. In fact, they correspond to the set of volume fraction profiles presented in Fig. 2 B and simultaneously reproduce all six reflectivity curves remarkably well. The only parameters that were allowed to vary between the two samples are those related to the transfer (f_{BL1}, f_{BL2}) and to the oxide layer on the solid substrate (d_{oxi}, $\phi_{\mathrm{W}}^{\mathrm{oxi}}$, $\sigma_{\mathrm{Si,oxi}}$, $\sigma_{\mathrm{oxi,W}}$), as these cannot be expected to be identical. It should be noted that two separate yet inconsistent fits of the two samples with h- and d-phospholipids would reproduce the data even slightly better, however at the cost of greater ambiguity. Moreover, the chosen "$\log(R \cdot q_z^4)$ vs. $\log(q_z)$" representation highlights deviations between fit and experimental data more

than the more commonly used "$\log(R)$ vs. q_z" representation. One possible reason for the remaining deviations between the global fits and the experimental data could be progressive variations of certain sample parameters (such as bilayer coverage) associated with slow defect healing between the measurements with different H_2O/D_2O mixtures. Additional data and fits for PC FLBs, PC/Trihexo FLBs, PC/LacCer FLBs and PC/GM1 FLBs are presented in the Supporting Information (Figs. S2-S5).

In most cases, the bilayer coverages after annealing by heating to 50°C were found to be excellent ($f_{\mathrm{BL}}^{\mathrm{prox}} \gtrsim 0.96$, $f_{\mathrm{BL}}^{\mathrm{dist}} \gtrsim 0.90$, see Table 2). In these cases, differences between the coherent and incoherent treatments of heterogeneities in the reflectivity modeling are small. We emphasize, however, that the treatment becomes important when the bilayer coverage is incomplete, as frequently observed for samples at 25°C prior to annealing (Table 3). In these cases, good agreement between experimental and modeled reflectivity curves was only achieved with the incoherent treatment, in line with the ellipsometry measurements, which suggest that heterogeneities are laterally macroscopic when occurring. By contrast, poor agreement was observed with the coherent treatment (see Supporting Information, Fig. S6). Based on the combined interpretation of ellipsometry and NR results we conclude that heterogeneities occurring during the LB/LS transfer of lipid bilayers onto solid surfaces may typically have macroscopic length scales and therefore may often have to be handled with an incoherent treatment, in contrast to the typical implementation in commonly used NR fitting packages. Note, however, that generality with regard to this conclusion cannot be claimed, although support can also be found in earlier reports with a more general perspective on deposition techniques and parameters.[50]

FLBs containing GM1 were found to be unstable, i.e., to lose their distal bilayers, even at the lowest glycolipid content ($x_{\mathrm{GL}}^{\mathrm{BL}} = 0.05$), even before heating the samples to 50°C (Tables 2 and 3), and even when their preparation was attempted in the presence of 100 mM NaCl. We attribute this result to the negative charge that GM1 is bearing in contrast to the other glycolipids investigated and that leads to electrostatic repulsion. In fact, a 5 mol% content of

negative lipids was previously reported to suppress multilamellar states of lipid membranes even in the presence of 100 mM salt.[14] We emphasize that this result is not in contradiction to earlier reports of attractive interactions between fully charged lipid bilayers[26] because the much lower charge densities relevant in the present work do not fall into the "strong coupling" regime in which attraction is expected.[51]

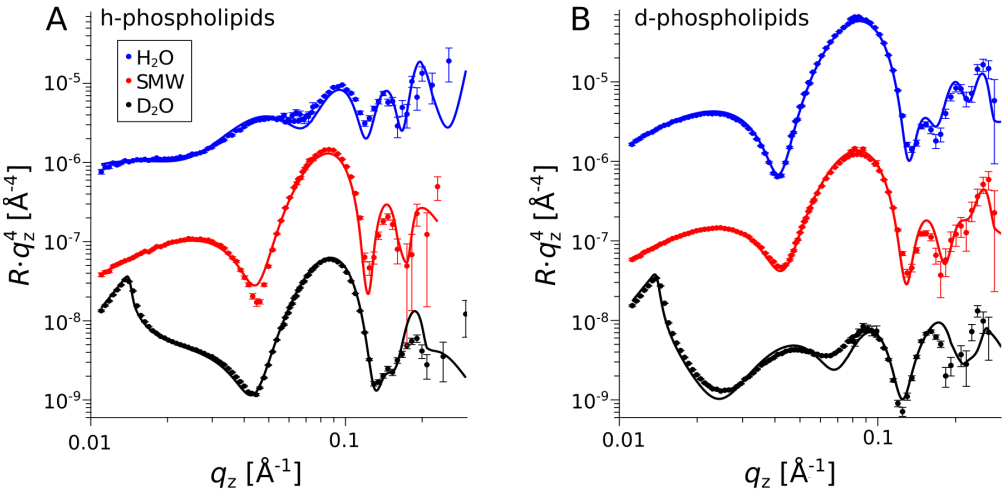

Figure 3: NR curves obtained at 50°C with a PC/Trihexo FLB. (A) Sample with chain-hydrogenous phospholipids. (B) Sample with chain-deuterated phospholipids. Solid lines: simulated reflectivity curves corresponding to a common volume fraction model reproducing all six reflectivity curves in panels A and B. This model is shown in Fig. 2 B.

Having assessed that PC FLBs, PC/Trihexo FLBs and PC/LacCer FLBs are stable even at high temperatures, we turn to the structural parameters obtained in the reflectivity analysis. The oxide layer parameters (mean ± standard deviation over all samples) were obtained as $d_{\mathrm{oxi}} = 9 \pm 1$ Å, $\phi_{\mathrm{W}}^{\mathrm{oxi}} = 0.08 \pm 0.06$, $\sigma_{\mathrm{Si,oxi}} = 3 \pm 1.5$ Å, and $\sigma_{\mathrm{oxi,W}} = 3 \pm 1$ Å, which is consistent with earlier works.[30,36] The water layer below the proximal bilayer was found to have a thickness of $d_{\mathrm{W}}^{\mathrm{SiBL}} \lesssim 5$ Å and an effective thickness including phospholipid headgroup hydration of $D_{\mathrm{W}}^{\mathrm{SiBL}} = d_{\mathrm{W}}^{\mathrm{SiBL}} + d_{\mathrm{HG}}\phi_{\mathrm{W}}^{\mathrm{HG}} = 4 \pm 1$ Å. With $2d_{\mathrm{HC}}^{\mathrm{prox}} = 39 \pm 1$ Å for both temperatures investigated, the hydrophobic thickness of the proximal bilayer is in good agreement with an earlier study,[52] but somewhat thinner than what was reported in two other studies.[27,28] In any case, it exactly matches the geometrical expectation:[53] $2d_{\mathrm{HC}} = 2 \cdot \left[1.54 \text{ Å} + 17 \cdot 1.27 \text{ Å}\right] \cdot \cos t \approx 39$ Å for phospholipids with C_{18} chains in a gel

phase with the reported tilt angle of $t \approx 33°$.[54] The roughness parameter characterizing its fluctuation amplitude was obtained as $\sigma_{\mathrm{fluc}}^{\mathrm{prox}} = 4 \pm 1$ Å, which is comparable to earlier reports.[27]

In the following we will focus the discussion on the results obtained at 50°C, where the distal bilayer is in the fluid phase. The most important parameters are summarized in Table 2. Selected parameters at 50°C are visualized in Fig. 4 for a comparison between the reference sample and samples containing the two glycolipid types that led to stable FLBs. A first observation is that the the hydrophobic thickness of the distal bilayer, $2d_{\mathrm{HC}}^{\mathrm{dist}} \approx 31$ Å, agrees well with earlier studies on fluid DPPC[27] and is almost unaffected by the glycolipids, in agreement with previous results on FLBs containing gangliosides.[29] Comparing $2d_{\mathrm{HC}}^{\mathrm{dist}}$ of the distal bilayer at 25°C and 50°C reveals a difference of about 4 Å on average (see Tables 2 and 3), confirming the occurrence of a phase transition between these temperatures. In contrast, no such thickness change occurs for the proximal bilayer (see Table S1 in the Supporting Information), in line with the expectation of a persistent chain-crystalline state. The presence of glycolipids does not have a significant influence on the hydrophobic thickness either, despite reports that glycolipids can affect the degree of ordering in lipid layers close to a phase transition.[18] Apparently, the temperatures chosen here are sufficiently far away from such a transition, so that the glycolipids have no significant effect. This result also confirms that the chain lengths of the glycolipids and the matrix phospholipids indeed match well and indicates that the glycolipids do not significantly alter the lipid packing of the bilayer in the fluid state. No significant influence of the glycolipids is observed for the headgroup layer thickness $d_{\mathrm{HG}}^{\mathrm{dist}}$ either. These results also serve as a-posteriori justification of the assumption of an approximately constant bilayer thickness that was made previously.[14]

Apart from the bilayer structure, the present work is also focused on the interactions occurring between the adjacent bilayers. These are reflected by the inter-bilayer distance and by the undulations of the fluid distal bilayer. For PC lipid bilayers, the equilibrium water layer thickness is largely governed by long-range van der Waals attraction and by what is com-

monly referred to as hydration repulsion.[13,55,56] The strength of the hydration repulsion is known to depend on the bilayer phase,[57] although its mechanisms it still under debate[9] and it is difficult to disentangle it from other (usually less dominant) repulsive contributions such as the undulation repulsion,[58] which depends on the bilayers' bending rigidity. The most robust quantity to look at for comparison with earlier studies is the effective water layer thickness including the headgroup hydration, $D_{\mathrm{W}} = d_{\mathrm{W}} + 2d_{\mathrm{HG}}\phi_{\mathrm{W}}^{\mathrm{HG}}$, because it is invariant to (sometimes ambiguous) details of the headgroup layer description. With $D_{\mathrm{W}} \approx 21$ Å (Table 2), the water layer between the bilayers of the PC FLB (one in the gel and one in the fluid state) is thinner than what was reported for two PC lipid bilayers in the fluid state (25-30 Å)[59,60] but also thicker than what was reported for two PC lipid bilayers in the gel state (15-20 Å)[59,60] in line with our result at 25°C, $D_{\mathrm{W}} \approx 18$ Å (Table 3). This finding may suggest that the hydration repulsion is of intermediate range and strength in non-symmetrical interaction scenarios, but more systematic investigations will be required to test this hypothesis.

Importantly, the water layer thickness (in terms of both d_{W} and D_{W}) exhibits a considerable response to the incorporation of 20 mol% Trihexo or LacCer (Fig. 4). While Trihexo increases D_{W} by about 1 Å, LacCer has the opposite effect and reduces D_{W} by about 2 Å, in good agreement with the trends observed previously with membrane multilayers.[14] The agreement also persists in a quantitative comparison on the level of lamellar periods d, which include the small contribution of bilayer thickness variations and can be constructed in the present study as $d = d_{\mathrm{W}} + 2(d_{\mathrm{HC}} + d_{\mathrm{HG}})$. We obtain $\Delta d \approx +3$ Å for Trihexo and $\Delta d \approx$ -1 Å for LacCer (see inset in Fig. 4), compared to $\Delta d \approx +2$ Å for Trihexo and $\Delta d \approx$ -3 Å for LacCer in the multilayer study. A similar trend is also observed at 25°C (Table 3). Here, we recall that the incorporation of glycolipids does not affect the bilayer thickness (Tables 2 and 3), so that a significant change in the bilayer bending is not expected. In fact, earlier neutron scattering experiments have shown that the addition of up to 25 % glycolipids even with pentasaccharide headgroups did not affect the bending modulus of fluid bilayers.[13] A

significant role of a change in the strength of the undulation repulsion for the equilibrium water layer thickness is therefore unlikely.

As suggested earlier,[13] one may expect that the length of two trans-engaged saccharide headgroups dictates the water layer thickness between bilayers displaying adhesion-promoting glycolipids. However, as shown more recently with the help of atomistic molecular dynamics simulations,[15] the formation of such trans-bonds requires significant overlap of the interacting saccharides and thus much smaller membrane separations that locally arise from thermal undulations of adjacent bilayers. In fact, in Fig. 2 B the volume fraction profiles of the headgroups belonging to the opposing bilayer surfaces exhibit a significant overlap despite the thick effective water layer. Note that the headgroup profiles reconstructed from the NR data only demonstrate that the headgroup layers as such overlap, which illustrates how close the proximity of the adjacent bilayers can locally be, a requirement for trans-engagement of saccharide headgroups. Due to the unified layer description of all headgroups in the NR data analysis (see Methods section), the profiles do not provide any information on the actual overlap of specifically the glycolipid headgroups.

In summary, what governs the change in the water layer thickness in the presence of the glycolipids must be considered the result of an antagonism between the steric repulsion induced by non-trans-engaged saccharide headgroups on thermally undulating bilayer surfaces and the effective attraction induced by the trans-engaged saccharide headgroups. The amplitude of the membrane roughness associated with the thermal undulations, $\sigma_{\rm fluc}^{\rm dist}$, is related to the membrane-membrane interaction potential.[25,61] For oriented multibilayers[62] the amplitude of collective fluctuations was previously reported to decrease with increasing density of glycolipids with adhesion-promoting saccharide headgroups.[13] Here, the presence of Trihexo or LacCer on the surfaces of the two interacting bilayers, despite the clear influence on $D_{\rm W}$, does not seem to have any significant influence on $\sigma_{\rm fluc}^{\rm dist}$ (see Fig. 4 and Table 2).

Whether or not the presence of Trihexo or LacCer results in more stable FLBs cannot be judged on the basis of the water layer thickness and roughness parameters alone. Alterna-

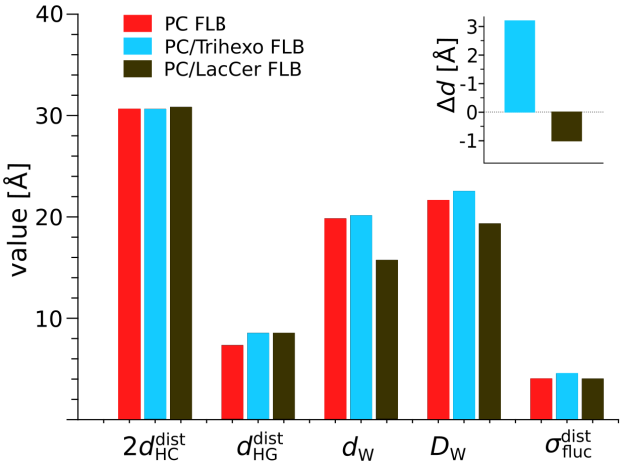

Figure 4: Parameters of the distal bilayer obtained in the analysis of NR curves measured with FLB samples at 50°C. Hydrophobic thickness: $2d_{\mathrm{HC}}^{\mathrm{dist}}$, headgroup layer thickness: $d_{\mathrm{HG}}^{\mathrm{dist}}$, water layer thickness: d_{W}, effective water layer thickness: D_{W}, amplitude of thermal undulations: $\sigma_{\mathrm{fluc}}^{\mathrm{dist}}$. Inset: Change Δd in the lamellar spacing induced by the presence of the glycolipids.

tively, the adhesion strength can be assessed by inducing an additional repulsive contribution to the interaction potential between the adjacent bilayers, in the spirit of earlier studies.[13,14] In the present work, we explored this possibility by rinsing the PC/Trihexo and PC/LacCer FLBs at 50°C with a salt solution (100 mN NaCl) loaded with 5 mM $CaCl_2$ (without changing pH). The reflectivity curves together with the fits are shown in Fig. 5 A. Fluid PC lipid bilayers are known to react to small calcium concentrations with a substantial water layer thickening[63] and were reported to react to 5 mM $CaCl_2$ in 100 mN NaCl with a water layer thickness increase by as much as 25 Å.[13,64] The reason is a preferential interaction of Ca^{2+} with the bilayer surfaces, which results in an effective surface charge and, in turn, in electric repulsion. Strikingly, the response of the water layer thickness to the addition of 5 mM $CaCl_2$ was found to be much smaller in the presence of adhesion-promoting glycolipids,[64] which was interpreted as result of the trans-engaged saccharide bonds. Here, the same concentration of $CaCl_2$ only leads to a moderate change ($\Delta d_{\mathrm{W}} \approx 7$ Å, see Fig. 5 B) for the PC/LacCer FLB and has almost no effect on the PC/Trihexo FLB ($\Delta d_{\mathrm{W}} \lesssim 1$ Å, see Fig. 5 B), which is comparable to earlier observations[13] made with the same $CaCl_2$ concentration with glycolipids bearing the adhesion-promoting Lewis^X trisaccharide at similar

glycolipid densities ($\Delta d_{\mathrm{W}} \approx 1$ Å at $x_{\mathrm{GL}}^{\mathrm{BL}} = 0.25$). The present results thus suggest that similar sugar-induced adhesion-strengthening also occurs in the glycolipid-containing FLBs investigated here. With that, we not only confirm the results of our previous work but also provide indications that LacCer and Trihexo glycolipids promote the adhesion between facing bilayers, even against imposed electrostatic repulsion. The role of sugars on the surfaces of biological membranes for cell adhesion is well known but direct quantitative investigations of their action is not straightforward. Here, we show that deeper insights can be gained from the impacts of temperature changes and salt addition. Moreover, by including selected glycolipids into FLBs and by exploiting the influences of temperature and salts, one can tune and stabilize the distance between adjacent bilayers, which opens up opportunities to investigate specific inter-membrane protein-protein, lipid-lipid, or protein-lipid binding at varying membrane separation.

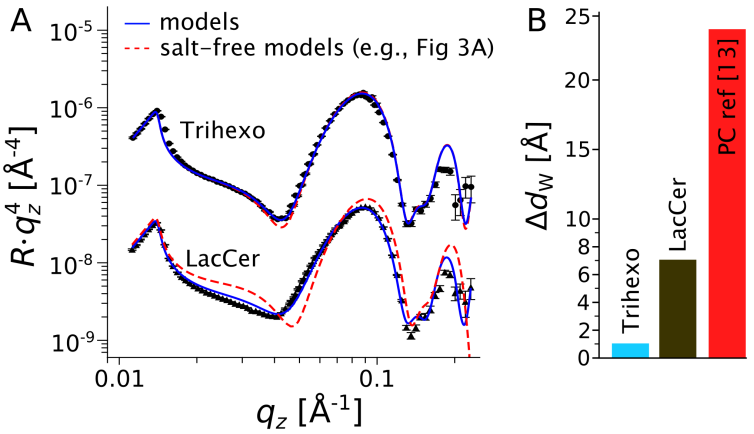

Figure 5: (A) NR curves after rinsing PC/Trihexo and PC/LacCer FLBs (all based on h-phospholipids) at 50°C with a salt solution loaded with 5 mM $CaCl_2$. Solid lines are fits to these data in which only d_W, $d_{\mathrm{HG}}^{\mathrm{dist}}$, and coverages were allowed to vary with regard to the original model (indicated with dashed lines). (B) Calcium-induced change Δd_{W} in the water layer thickness for FLBs containing glycolipids (this work) and in pure PC lipid multilayers (ref[13]).

Another interesting aspect that can be profitably investigated with NR from FLBs is the distribution of glycolipids between the two leaflets of the interacting bilayers. Since the proximal bilayer remains in the chain-ordered gel phase at all times, exchange of glycolipids between its two leaflets can be safely neglected and the glycolipid fraction remains at the

Table 2: Best-matching model parameters obtained in the analysis of neutron reflectivity curves measured with FLB samples at 50°C. [a]Data range insufficient for full analysis because only small q_z-range was measured when absence of second bilayer ways obvious.

FLB sample	x_{GL}^{BL}	T [°C]	h/d	f_{BL}^{prox}; f_{BL}^{dist} ($\pm$0.05)	$2d_{HC}^{dist}$; d_{HG}^{dist} [Å] ($\pm$1)	d_W; D_W [Å] ($\pm$1)	σ_{fluc}^{dist} [Å] ($\pm$1)	f_{in} ($\pm$0.05)
PC	0.20	50	h	0.96; 0.96	31; 7	20; 22	4	-
PC/Trihexo	0.20	50	h	1.00; 0.98	31; 9	20; 23	5	0.46
			d	1.00, 0.92				
PC/LacCer	0.20	50	h	1.00; 0.96	31; 9	16; 19	4	0.40
			d	0.99; 0.90				
PC/GM1	0.10	50	h	-[a]; -	-; -	-; -	-	-
	0.05	50	h	-[a]; -	-; -	-; -	-	-

Table 3: Best-matching model parameters obtained in the analysis of neutron reflectivity curves measured with FLB samples at 25°C. [b]Fixed as imposed by the preparation.

FLB sample	x_{GL}^{BL}	T [°C]	h/d	f_{BL}^{prox}; f_{BL}^{dist} ($\pm$0.05)	$2d_{HC}^{dist}$; d_{HG}^{dist} [Å] ($\pm$1)	d_W; D_W [Å] ($\pm$1)	σ_{fluc}^{dist} [Å] ($\pm$1)	f_{in}
PC	0	25	h	0.98; 0.74	34; 8	15; 18	5	-
PC/Trihexo	0.20	25	h	0.88; 0.88	36; 10	17; 20	4	0.5[b]
			d	0.89; 0.50				
PC/LacCer	0.20	25	h	0.92; 0.91	36; 9	13; 16	3	0.5[b]
			d	1.00; 0.67				
PC/GM1	0.10	25	h	0.93; -	-; -	-; -	-	-
	0.05	25	h	0.90; -	-; -	-; -	-	-

initial value of $x_{\mathrm{GL}}^{\mathrm{BL}}$ in the outer leaflet. In contrast, when the sample is heated to 50°C across the distal bilayer's melting temperature, the glycolipids in this bilayer may have the possibility to change leaflet through flip-flop or other processes to the same effect. One may expect, for example, that favorable interactions between the glycolipids on the surfaces of the two adjacent bilayers promote glycolipid enrichment on the inner leaflet of the distal bilayer. As described in the Methods section, one fit parameter (f_{in}) was the glycolipid distribution over the two leaflets. The reflectivity curves of the samples prepared with d-phospholipids are very sensitive to this parameter because the deuterated phospholipid tails have an enormous SLD contrast against the non-deuterated ("hydrogenous") glycolipid tails. Fig. 6 A shows these reflectivity curves for a d-phospholipid-based PC/Trihexo FLB measured at 50°C, together with the simulated curves for different values of f_{in}. The best match (solid lines) is obtained for $f_{\mathrm{in}} = 0.46$ (see Table 2), which means that, within the experimental uncertainty, the glycolipids remain evenly distributed over the two leaflets. The dashed lines indicate the simulated curves for $f_{\mathrm{in}} = 1$, a hypothetical scenario in which all glycolipids accumulate in the inner leaflet. The SLD profiles corresponding to the two scenarios for all three H_2O/D_2O mixtures are shown in Fig. 6 B. Clearly, any substantial accumulation in the inner leaflet is ruled out by the strong deviation of the corresponding simulated reflectivity curves from the experimental ones (Fig. 6 A). A similar result is also obtained for the PC/LacCer FLB (see Table 2). Here, the fit result of $f_{\mathrm{in}} = 0.40$ even seems to indicate a tendency for glycolipid accumulation in the outer (non-interacting) leaflet, however the observed deviation from an even distribution ($f_{\mathrm{in}} = 0.5$) appears to be at the limit of statistical significance.

We consider two reasons for the glycolipids to remain evenly distributed over the two leaflets. The first is that the glycolipids are unable to undergo flip-flop on the time scale of the experiment. Indeed, while phospholipids can be subject to rapid flip-flop in fluid bilayers,[47] flip-flop of charged glycolipids with large headgroups was reported not to occur.[46] However, LacCer and Trihexo are much more compact and uncharged, so that the barrier to undergo flip-flop can be considered much lower. The factors relevant for flip-flop rates have previously

been addressed with coarse-grained molecular dynamics simulations.[65] The second potential reason for evenly distributed glycolipids could be the absence of a sufficiently strong driving force for redistribution. If, for example, only a small fraction of the glycolipids were engaged in a trans-bond of low binding free energy, as suggested earlier,[15] then likely no significant redistribution will occur. Finally, if the slight accumulation on the outer surface were real, it would require that there is a certain driving force for this process, such as steric exclusion of the glycolipid headgroups from the thin water layer. In this case, the driving force should be stronger for the bulkier Trihexo headgroup, but at the same time this molecule likely has the higher barrier to flip-flop.

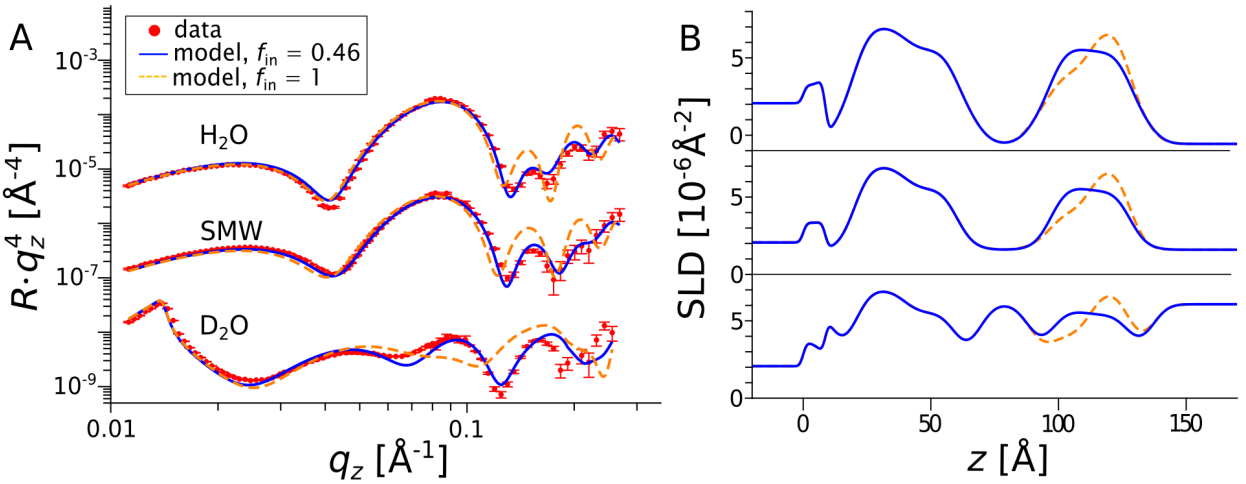

Figure 6: (A) NR curves for a d-phospholipid-based PC/Trihexo FLB measured at 50°C, together with the simulated curves for $f_{in} = 0.46$ (approximately even glycolipid distribution) and for $f_{in} = 1$ (glycolipid accumulation in the inner leaflet). (B) SLD profiles corresponding to these two scenarios.

Conclusions

FLBs containing defined fractions of various types of glycolipids were prepared through the sequential deposition of four lipid monolayers onto initially bare silicon surfaces. In most cases, the bilayer coverages after heating to 50°C were found to be excellent. For the other cases, the ellipsometry and NR results indicate that heterogeneities have macroscopic length

scales and therefore should be handled with an incoherent treatment of the NR data. The studied glycolipids have a distinct influence on the inter-bilayer water layer thickness, in line with the results of earlier studies on lipid-multibilayers. In tendency, the addition of suitable glycolipids seems to contribute to the stability of the FLBs: the layers have excellent coverage, remain highly organized also above the melting transition, and do not exhibit much of a calcium-induced water-layer thickening, which is in contrast to pure PC lipid membranes. Despite the well-documented preferential interactions between their saccharide headgroups across the water layer, the glycolipids do not accumulate on the face of the bilayer that is in contact with the saccharide-bearing supporting bilayer. This may have to do with their inability to perform flip-flop or with an insufficient driving force for such a redistribution.

The possibility of creating stable FLBs mimicking two interacting sugar-exposing plasma membranes enables one to investigate a variety of interesting phenomena occurring at cell surfaces. One could, for example, study the role of free macromolecules in cell adhesion. Tuning the inter-bilayers distance with small fractions of suitable glycolipids may further allow to investigate direct interactions among molecules included in the two facing membranes, such as specific lipid and protein interactions. Indeed, investigating direct interactions among membrane components has remained challenging despite existing protocols for the study of protein-ligand interactions.[66] Deviations in the distance between plasma membranes have also been associated with the health state of cells, for example in breast cancer.[67] The sample architectures and analysis methods described in the present work may be suitable for the study of such phenomena.

Supporting Information

Calculation of glycolipid headgroup volumes and SLDs; Influence of $\sigma_{\mathrm{fluc}}^{\mathrm{prox}}$ and $\sigma_{\mathrm{fluc}}^{\mathrm{dist}}$ on the volume fraction profiles; Additional NR data and fits; Coherent vs. incoherent treatment of FLBs with incomplete coverage; Hydrophobic thickness of the proximal bilayer at 25°C and

50°C; Influence of an independent thickness parameter for the GHG distribution; Additional ellipsometry data.

Conflicts of Interest

There are no conflicts of interest to declare.

Acknowledgement

The authors wish to thank Philipp Gutfreund for help with the neutron reflectometry experiments and the Institut Laue-Langevin in Grenoble (FR) for beamtime and use of the facilities offered by the Partnership for Soft Condensed Matter (PSCM). The raw data of the experiments can be found at https://doi.ill.fr/10.5291/ILL-DATA.8-02-966. E.S. gratefully acknowledges financial support by the German Research Foundation (DFG) via grant SCHN 1396/2 and V.R. gratefully acknowledges financial support by Ministero Italiano dell'Istruzione e del Merito (MUR) in the frame of PRIN2020 grants, grant number 2020MHL8S9.

References

(1) Simons, K.; Ikonen, E. Functional rafts in cell membranes. *Nature* **1997**, *387*, 569–572.

(2) Van Meer, G.; Voelker, D. R.; Feigenson, G. W. Membrane lipids: where they are and how they behave. *Nature reviews Molecular cell biology* **2008**, *9*, 112–124.

(3) Boudière, L.; Michaud, M.; Petroutsos, D.; Rébeillé, F.; Falconet, D.; Bastien, O.; Roy, S.; Finazzi, G.; Rolland, N.; Jouhet, J.; Block, M. A.; Maréchal, E. Glycerolipids in photosynthesis: composition, synthesis and trafficking. *Biochimica et Biophysica Acta (BBA)-Bioenergetics* **2014**, *1837*, 470–480.

(4) Jala, R. C. R.; Vudhgiri, S.; Kumar, C. G. A comprehensive review on natural occurrence, synthesis and biological activities of glycolipids. *Carbohydrate Research* **2022**, 108556.

(5) Bucior, I.; Scheuring, S.; Engel, A.; Burger, M. M. Carbohydrate–carbohydrate interaction provides adhesion force and specificity for cellular recognition. *The Journal of cell biology* **2004**, *165*, 529–537.

(6) Bucior, I.; Burger, M. M. Carbohydrate-carbohydrate interaction as a major force initiating cell-cell recognition. *Glycoconjugate Journal* **2004**, *21*, 111–123.

(7) Ryrif, I. J.; Anderson, J. M.; Goodchild, D. J. The role of the light-harvesting chlorophyll a/b-protein complex in chloroplast membrane stacking: Cation-induced aggregation of reconstituted proteoliposomes. *European Journal of Biochemistry* **1980**, *107*, 345–354.

(8) Webb, M. S.; Green, B. R. Effects of neutral and anionic lipids on digalactosyldiacylglycerol vesicle aggregation. *Biochimica et Biophysica Acta (BBA)-Biomembranes* **1990**, *1030*, 231–237.

(9) Kanduč, M.; Schlaich, A.; de Vries, A. H.; Jouhet, J.; Demé, B.; Netz, R. R.; Schneck, E. Tight cohesion between glycolipid membranes results from balanced water–headgroup interactions. *Nat. Comm.* **2017**, *8*.

(10) Pincet, F.; Le Bouar, T.; Zhang, Y.; Esnault, J.; Mallet, J.-M.; Perez, E.; Sinay, P. Ultraweak sugar-sugar interactions for transient cell adhesion. *Biophysical Journal* **2001**, *80*, 1354–1358.

(11) Gourier, C.; Pincet, F.; Perez, E.; Zhang, Y.; Mallet, J.-M.; Sinaÿ, P. Specific and non specific interactions involving Le X determinant quantified by lipid vesicle micromanipulation. *Glycoconjugate Journal* **2004**, *21*, 165–174.

(12) Yu, Z.; Calvert, T.; Leckband, D. Molecular forces between membranes displaying neutral glycosphingolipids: evidence for carbohydrate attraction. *Biochemistry* **1998**, *37*, 1540–1550.

(13) Schneck, E.; Demé, B.; Gege, C.; Tanaka, M. Membrane Adhesion via homophilic saccharide-saccharide interactions investigated by neutron scattering. *Biophysical Journal* **2011**, *100*, 2151–2159.

(14) Latza, V. M.; Demé, B.; Schneck, E. Membrane adhesion via glycolipids occurs for abundant saccharide chemistries. *Biophysical Journal* **2020**, *118*, 1602–1611.

(15) Kav, B.; Grafmüller, A.; Schneck, E.; Weikl, T. R. Weak carbohydrate–carbohydrate interactions in membrane adhesion are fuzzy and generic. *Nanoscale* **2020**, *12*, 17342–17353.

(16) Sillerud, L. O.; Schafer, D. E.; Yu, R. K.; Konigsberg, W. H. Calorimetric properties of mixtures of ganglioside GM1 and dipalmitoylphosphatidylcholine. *Journal of Bioogial Chemistry* **1979**, *254*, 10876–10880.

(17) Watkins, E. B.; Frey, S. L.; Chi, E. Y.; Cao, K. D.; Pacuszka, T.; Majewski, J.; Lee, K. Y. C. Enhanced ordering in monolayers containing glycosphingolipids: Impact of carbohydrate structure. *Biophysical journal* **2018**, *114*, 1103–1115.

(18) Mukhina, T.; Brezesinski, G.; Shen, C.; Schneck, E. Phase behavior and miscibility in lipid monolayers containing glycolipids. *Journal of Colloid and Interface Science* **2022**, *615*, 786–796.

(19) Rondelli, V.; Mollica, L.; Koutsioubas, A.; Nasir, N.; Trapp, M.; Deboever, E.; Brocca, P.; Deleu, M. Carbohydrate-carbohydrate interaction drives the preferential insertion of dirhamnolipid into glycosphingolipid enriched membranes. *Journal of Colloid and Interface Science* **2022**, *616*, 739–748.

(20) Spangler, B. D. Structure and function of cholera toxin and the related escherichia coli heat-labile enterotoxin. *Microbiological Reviews* **1992**, *54*, 622–644.

(21) Lopez, P. H. H.; Schnaar, R. L. Gangliosides in cell recognition and membrane protein regulation. *Current Opinion in Structural Biology* **2009**, *19*, 549–557.

(22) Sipione, S.; Monyror, J.; Galleguillos, D.; Steinberg, N.; Kadam, V. Gangliosides in the brain: physiology, pathophysiology and therapeutic applications. *Frontiers in Neuroscience* **2020**, *14*, 572965.

(23) Schneck, E.; Rehfeldt, F.; Oliveira, R. G.; Gege, C.; Demé, B.; Tanaka, M. Modulation of intermembrane interaction and bending rigidity of biomembrane models via carbohydrates investigated by specular and off-specular neutron scattering. *Physical Review E* **2008**, *78*, 061924.

(24) Wacklin, H. P. Neutron reflection from supported lipid membranes. *Current Opinion in Colloid & Interface Science* **2010**, *15*, 445–454.

(25) Fragneto, G.; Charitat, T.; Daillant, J. Floating lipid bilayers: models for physics and biology. *European Biophysics Journal* **2012**, *41*, 863–874.

(26) Mukhina, T.; Hemmerle, A.; Rondelli, V.; Gerelli, Y.; Fragneto, G.; Daillant, J.; Charitat, T. Attractive interaction between fully charged lipid bilayers in a strongly confined geometry. *The Journal of Physical Chemistry Letters* **2019**, *10*, 7195–7199.

(27) Rondelli, V.; Del Favero, E.; Brocca, P.; Fragneto, G.; Trapp, M.; Mauri, L.; Ciampa, M. G.; Romani, G.; Braun, C. J.; Winterstein, L.; Schroeder, I.; Thiel, G.; Moroni, A.; Cantu, L. Directional K+ channel insertion in a single phospholipid bilayer: Neutron reflectometry and electrophysiology in the joint exploration of a model membrane functional platform. *Biochim Biophys Acta Gen Subj* **2018**, *1862*, 1742–1750.

(28) Rondelli, V.; Del Favero, E.; Motta, S.; Cantù, L.; Fragneto, G.; Procca, P. Neutrons for rafts, rafts for neutrons. *The European Physical Journal E* **2013**, *36*, 1–8.

(29) Rondelli, V.; Brocca, P.; Tranquilli, N.; Fragneto, G.; Del Favero, E.; Cantù, L. Building a biomimetic membrane for neutron reflectivity investigation: Complexity, asymmetry and contrast. *Biophysical Chemistry* **2017**, *229*, 135–141.

(30) Rodriguez-Loureiro, I.; Scoppola, E.; Bertinetti, L.; Barbetta, A.; Fragneto, G.; Schneck, E. Neutron reflectometry yields distance-dependent structures of nanometric polymer brushes interacting across water. *Soft Matter* **2017**, *13*, 5767–5777.

(31) Azzam, R. M.; Bashara, N. M.; Ballard, S. S. Ellipsometry and polarized light. *Physics Today* **1978**, *31*, 72.

(32) Adachi, S. Model dielectric constants of Si and Ge. *Physical Review B* **1988**, *38*, 12966.

(33) Ruths, J.; Essler, F.; Decher, G.; Riegler, H. Polyelectrolytes I: polyanion/polycation multilayers at the air/monolayer/water interface as elements for quantitative polymer adsorption studies and preparation of hetero-superlattices on solid surfaces. *Langmuir* **2000**, *16*, 8871–8878.

(34) Wong, J. E.; Rehfeldt, F.; Hänni, P.; Tanaka, M.; Klitzing, R. v. Swelling behavior of polyelectrolyte multilayers in saturated water vapor. *Macromolecules* **2004**, *37*, 7285–7289.

(35) Campbell, R.; Wacklin, H.; Sutton, I.; Cubitt, R.; Fragneto, G. FIGARO: The new horizontal neutron reflectometer at the ILL. *The European Physical Journal Plus* **2011**, *126*, 1–22.

(36) Latza, V. M.; Rodriguez-Loureiro, I.; Fragneto, G.; Schneck, E. End point versus backbone specificity governs characteristics of antibody binding to poly (ethylene glycol) brushes. *Langmuir* **2018**, *34*, 13946–13955.

(37) Dabkowska, A. P.; Talbot, J. P.; Cavalcanti, L.; Webster, J. R.; Nelson, A.; Barlow, D. J.; Fragneto, G.; Lawrence, M. J. Calcium mediated interaction of calf-thymus DNA with monolayers of distearoylphosphatidylcholine: a neutron and X-ray reflectivity study. *Soft Matter* **2013**, *9*, 7095–7105.

(38) Rodriguez-Loureiro, I.; Latza, V. M.; Fragneto, G.; Schneck, E. Conformation of single and interacting lipopolysaccharide surfaces bearing O-side chains. *Biophysical Journal* **2018**, *114*, 1624–1635.

(39) Petrache, H. I.; Tristram-Nagle, S.; Nagle, J. F. Fluid phase structure of EPC and DMPC bilayers. *Chemistry and Physics of Lipids* **1998**, *95*, 83–94.

(40) Koutsioumpas, A. Combined coarse-grained molecular dynamics and neutron reflectivity characterization of supported lipid membranes. *The Journal of Physical Chemitry B* **2016**, *120*, 11474–11483.

(41) Molinspiration Cheminformatics free web services, https://www.molinspiration.com, Slovensky Grob, Slovakia.

(42) Boretta, M.; Cantu, L.; Corti, M.; Del Favero, E. Cubic phases of gangliosides in water: possible role of the conformational bistability of the headgroup. *Physica A: Statistical Mechanics and its Applications* **1997**, *236*, 162–176.

(43) Pusterla, J.; Scoppola, E.; Appel, C.; Mukhina, T.; Shen, C.; Brezesinski, G.; Schneck, E. Characterization of lipid bilayers adsorbed to functionalized air/water interfaces. *Nanoscale* **2022**, *14*, 15048–15059.

(44) Parratt, L. G. Surface studies of solids by total reflection of X-rays. *Physical Review* **1954**, *95*, 359.

(45) Bevington, P. R.; Robinson, D. K.; Blair, J. M.; Mallinckrodt, A. J.; McKay, S. Data

reduction and error analysis for the physical sciences. *Computers in Physics* **1993**, *7*, 415–416.

(46) Rondelli, V.; Fragneto, G.; Motta, S.; Del Favero, E.; Brocca, P.; Sonnino, S.; Cantù, L. Ganglioside GM1 forces the redistribution of cholesterol in a biomimetic membrane. *Biochimica et Biophysica Acta (BBA)-Biomembranes* **2012**, *1818*, 2860–2867.

(47) Sperotto, M. M.; Ferrarini, A. Spontaneous lipid flip-flop in membranes: A still unsettled picture from experiments and simulations. *The Biophysics of Cell Membranes Book* **2017**, *19*, 29–60.

(48) Wu, H.-L.; Tong, Y.; Peng, Q.; Li, N.; Ye, S. Phase transition behaviors of the supported DPPC bilayer investigated by sum frequency generation (SFG) vibrational spectroscopy and atomic force microscopy (AFM). *Physicla Chemistry Chemical Physics* **2016**, *18*, 1411–1421.

(49) Fragneto, G.; Charitat, T.; Bellet-Amalric, E.; Cubitt, R.; Graner, F. Swelling of Phospholipid Floating Bilayers: The Effect of Chain Length. *Langmuir 19*.

(50) Kirniwan, J.; de Souza, J. F. V.; Dang, A. T.; Liu, G.-y.; Kuhl, T. L. Preparation and Characterization of Solid-Supported Lipid Bilayers Formed by Langmuir–Blodgett Deposition: A Tutorial. *Langmuir* **2018**, *34*, 15622–15639.

(51) Netz, R. R. Electrostatistics of counter-ions at and between planar charged walls: From Poisson-Boltzmann to the strong-coupling theory. *The European Physical Journal E* **2001**, *5*, 557–574.

(52) Charitat, T.; Bellet-Amalric, E.; Fragneto, G.; Graner, F. Adsorbed and free lipid bilayers at the solid-liquid interface. *The European Physical Journal B-Condensed Matter and Complex Systems* **1999**, *8*, 583–593.

(53) Israelachvili, J. N. *Intermolecular and surface forces*; Academic press, 2015.

(54) Tristram-Nagle, S.; Zhang, R.; Suter, R.; Worthington, C.; Sun, W.; Nagle, J. Measurement of chain tilt angle in fully hydrated bilayers of gel phase lecithins. *Biophysical Journal* **1993**, *64*, 1097–1109.

(55) Demé, B.; Dubois, M.; Zemb, T. Swelling of a lecithin lamellar phase induced by small carbohydrate solutes. *Biophysical journal* **2002**, *82*, 215–225.

(56) Leontidis, E.; Aroti, A.; Belloni, L.; Dubois, M.; Zemb, T. Effects of monovalent anions of the Hofmeister series on DPPC lipid Bilayers part II: Modeling the perpendicular and lateral equation-of-state. *Biophysical journal* **2007**, *93*, 1591–1607.

(57) Kowalik, B.; Schlaich, A.; Kanduc, M.; Schneck, E.; Netz, R. R. Hydration repulsion difference between ordered and disordered membranes due to cancellation of membrane–membrane and water-mediated interactions. *The Journal of Physical Chemistry Letters* **2017**, *8*, 2869–2874.

(58) Helfrich, W. Elastic properties of lipid bilayers: theory and possible experiments. *Zeitschrift für Naturforschung c* **1973**, *28*, 693–703.

(59) Lis, L.; McAlister, D.; Fuller, N.; Rand, R.; Parsegian, V. Interactions between neutral phospholipid bilayer membranes. *Biophysical Journal* **1982**, *37*, 657–665.

(60) Nagle, J. F.; Tristram-Nagle, S. Structure of lipid bilayers. *Biochimica et Biophysica Acta (BBA)-Reviews on Biomembranes* **2000**, *1469*, 159–195.

(61) Daillant, J.; Bellet-Amalric, E.; Braslau, A.; Charitat, T.; Fragneto, G.; Graner, F.; Mora, S.; Rieutord, F.; Stidder, B. Structure and fluctuations of a single floating lipid bilayer. *Proceedings of the National Academy of Sciences* **2005**, *102*, 11639–11644.

(62) Salditt, T. Thermal fluctuations and stability of solid-supported lipid membranes. *Journal of Physics: Condensed Matter* **2005**, *17*, R287.

(63) Lotan, O.; Fink, L.; Shemesh, A.; Tamburu, C.; Raviv, U. Critical conditions for adsorption of calcium ions onto dipolar lipid membranes. *The Journal of Physical Chemistry A* **2016**, *120*, 3390–3396.

(64) Kav, B.; Demé, B.; Gege, C.; Tanaka, M.; Schneck, E.; Weikl, T. R. Interplay of trans-and cis-interactions of glycolipids in membrane adhesion. *Frontiers in Molecular Biosciences* **2021**, *8*, 754654.

(65) Miettinen, M. S.; Lipowsky, R. Bilayer membranes with frequent flip-flops have tensionless leaflets. *Nano Letters* **2019**, *19*, 5011–5016.

(66) Gavutis, M.; Lata, S.; Piehler, J. Probing 2-dimensional protein–protein interactions on model membranes. *Nature Protocols* **2006**, *1*, 2091–2103.

(67) Palamidessi, A. et al. Unjamming overcomes kinetic and proliferation arrest in terminally differentiated cells and promotes collective motility of carcinoma. *Nature Materials* **2019**, *18*, 1252–1263.